Multi-arm Robotic Swimmer Actuated by Antagonistic SMA Springs

Michael Sfakiotakis, Asimina Kazakidi, Theodoros Evdaimon, Avgousta Chatzidaki and Dimitris P. Tsakiris

***Abstract*— The present paper considers the modeling, control, development and experimental validation of bio-inspired multi-arm underwater robotic swimmers actuated by compliant actuating elements, in the context of the soft robotics paradigm. Each one of the swimmer's compliant arms is actuated at its base by a pair of antagonistic compliant shape memory alloy (SMA) springs. The base joint of each such arm displays hysteretic behavior and asymmetries, which are compensated via the modified Prandtl-Ishlinskii (MPI) model of the joint's response, in conjunction with angular position feedback from a potentiometer. This closed-loop control scheme achieves fast and efficient tracking of a sculling joint motion profile. Experimental results based on a pair of such submerged arms, integrated in a catamaran hull, indicate the feasibility of this actuation and control scheme, providing propulsive speeds up to approximately 0.5 arm lengths per second ($\sim$50 mm/sec) and propulsive forces up to 30 mN. The experimental studies presented, regarding the effect of the arm kinematic parameters on propulsive speed and force, are in qualitative agreement with previous results of our group for rigid-actuator multi-arm underwater swimmers.**

***Index Terms*— Bio-Inspired Robotics, Soft Robotics, Marine Robotics, Shape Memory Alloys, Control, Prandtl-Ishlinskii model.**

I. INTRODUCTION

The exploitation of soft components on sophisticated robotic systems can greatly enhance their manipulation and locomotion capabilities, offering solutions to robotic applications in complex environments [1]. Shape Memory Alloys (SMA) have been commonly used, in recent years, as compliant actuation structures on soft robots. The advantages of SMAs lie on the material's characteristics, being lightweight, small, simple in design and quiet in operation [2], [3]. Nickel-Titanium (Ni-Ti) SMA actuators have, further, the advantage of being highly ductile, reversible, corrosion resistant, highly bio-compatible, and easily electrically heated. The increased energy density of SMAs allows for the use of such actuators on reduced size systems; their structure can be configured into springs that intensify their stroke [4].

The use of compliant SMA actuators in robotics is gaining increasing popularity against rigid servomotors, in particular for biologically-inspired systems, aiming, for example, at emulating the efficiency of animal muscles, for both terrestrial [5]–[8] and aquatic locomotion [9]–[11].

Known challenges associated with SMA actuation relate primarily to their control precision, that requires compensation of several nonlinear effects, in order to avoid undesirable dynamical phenomena, instabilities in the system, or performance tracking difficulties. Such nonlinearities are predominantly due to the material's complex hysteretic behavior, which, in turn, is related to the shape memory characteristic of the SMA. Another limitation of the control of SMAs is the requirement for low-bandwidth operation, which is due to their slow response time during the cooling transition.

Within this framework, this paper discusses a closed-loop control strategy for rotary joints actuated by an antagonistic pair of SMA springs, and presents proof-of-concept design and experimental results of a two-arm planar swimmer with soft arms and actuation. The control scheme incorporates the inverse of the modified Prandtl-Ishlinski model [12] of the system's response as a feedforward term for hysteresis and asymmetry compensation, along with a feedback controller, to achieve effective tracking of the reference angular position. The proposed scheme is found to be effective in reduced size systems, with moderate to low computational effort.

The effect of a soft body on a multi-arm underwater robot has been recently presented in [13]–[17], for designs inspired by the octopus morphology. These soft-body robots employ eight compliant arms and a passively-compliant web, but use rigid actuators (micro-servomotors). The corresponding model includes information from detailed hydrodynamic studies [18]–[21] and is in accordance with relevant elastodynamic investigations of octopus arm muscle activation [22], [23]. These prototypes have demonstrated forward and turning propulsion with sculling-only gaits, achieving speeds of up to 0.5 body lengths per second with the web, and maximum propulsive forces of 10.5 N, with a cost of transport as low as 0.62 [14]; they have also been tested for grasping capabilities and suitability in a marine ecosystem [13].

The aim of the present paper is to extend these previous studies by incorporating soft actuation by SMA springs, in place of the rigid servos, and, thus, reducing the size of the robot swimmers. The speed and accuracy of the arm motion, which can be achieved with such actuators, is significantly ameliorated by employing closed-loop control of the SMAs. Indeed, open-loop control of the SMAs induces scaling and delaying effects to their response when tracking a desired joint arm trajectory (in particular, the "sculling" profile used in [13]), which are improved by our closed-loop scheme.

Section II of the paper presents a methodology for the

This work was supported in part by the European Commission (EC), the EC/ERDF and the GSRT of the Hellenic Ministry of Education via the BIOSYS-KRIPIS project [MIS-448301 (2013SE01380036)], by the ESF-GSRT HYDRO-ROB Project [PE7(281)], as well as by Greek national funds through the Operational Program "Education and Lifelong Learning" of the National Strategic Reference Framework - Research Funding Program: THALES via the BioLegRob Project (Mis: 379424).

The authors are with the Institute of Computer Science, Foundation for Research and Technology – Hellas (FORTH), Heraklion, Greece. M. Sfakiotakis is also with the Dept. of Electrical Engineering, Technological Educational Institute of Crete, Heraklion, Greece. {sfakios, kazakidi, evdemon, avgousta, tsakiris}@ics.forth.gr.

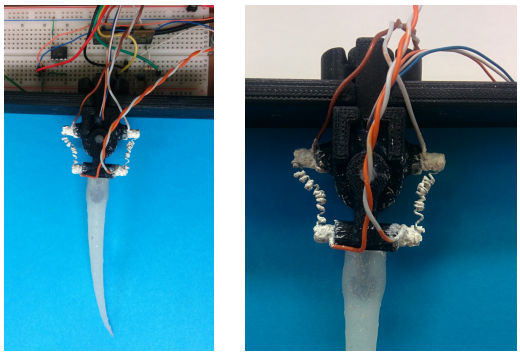

Fig. 1: The SMA-actuated 1-dof revolute joint.

closed-loop control of a rotary joint actuated by an antagonistic pair of SMA springs, and its experimental validation using a single-joint testbed. Section III presents the modeling and CFD studies, and the design of a proof-of-concept prototype SMA-actuated robotic swimmer, with two arms actuated by pairs of SMA springs and whose control is based in the above methodology, as well as associated experimental studies. Finally, Section IV summarizes the results of this work, and discusses its impact.

II. CONTROL OF SMA-ACTUATED JOINTS

A. SMA-actuated arm and control methodology

The 1-dof rotary joint prototype arm, employed in the current work, is shown in Fig. 1. Two identically "trained" SMA springs, positioned symmetrically on the lateral sides of the joint in an antagonistic configuration, allow bidirectional actuation of the soft arm in the transverse plane, achieving a 40° span of rotation. The SMAs, made of $250\,\mu$m-diameter NiTi wire (Flexinol, Dynalloy Inc.), were first wrapped tightly around a $2\,$mm rod to form them into coils of $5\,$mm in length (which correspond to $73\,$mm length of uncoiled NiTi wire), before being heated in an oven at $450\,^\circ$C, for $20\,$min, and then cooled down with water outside the oven. This process trains the SMAs to remember the shape of the coil and to revert to this shape upon heating, after being deformed. In order to allow underwater operation of the joint, the actuator SMA springs are coated with Teflon. A rotary potentiometer, mounted on the joint, is utilized to provide feedback for its angular position. A CortexM4-based microcontroller platform (Teensy 3.1) is used to control the prototype, by collecting the potentiometer's signal with an on-board 12-bit A/D converter, and generating PWM signals for the regulation of the SMAs electrical power supply from a $7.4\,$V source, via a pair of IRFZ44 mosfets.

The SMA-actuated arm is made of soft silicone rubber (Dragon Skin Q), taking on a conical shape with $10\,$mm in base diameter, $1\,$mm in tip diameter, and $100\,$mm in length. The shape of the arm is chosen to emulate the octopus arms, as described in [14]–[18], [21].

The implemented strategy for the joint actuation in the experimental prototype, based on the antagonistic activation of the two SMA springs, is depicted in Fig. 2. Turning moments are produced through the force generated by the SMA spring in the corresponding side, as it contracts through

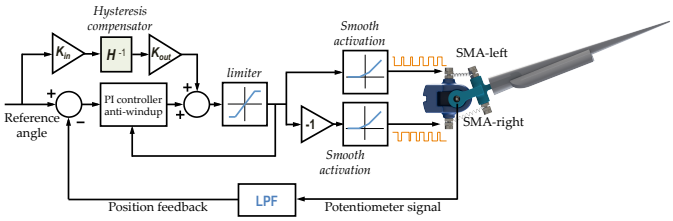

Fig. 2: The combined closed-loop feedforward-feedback position control scheme, developed for the SMA-actuated joint.

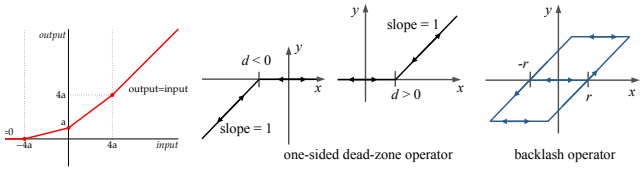

Fig. 3: (a) Input-output characteristics of the "smooth activation" modules. (b) Elementary operators employed in the MPI hysteresis models.

PWM- regulated electrical heating. Being related to the duty cycle of the PWM signals generated by the microcontroller, the range of the SMA activation command signal is -100% to 100%, where its sign denotes the desired turning direction (and, hence, which of the two SMA springs will be activated), while its magnitude affects the extent of the turning motion. The duty cycle of PWM signals originates from "smooth activation" modules that allow the SMAs to change smoothly between heated and non-heated states [24]. Figure 3a depicts the input-output characteristic of these modules, the transition phase of which is large enough to allow preheating of the opposite SMA, and therefore reduction of the response time for a nearly zero control signal. Here, we assumed a transition phase of $[-4a, 4a]$, where a is equal to 4% of the control input maximum value.

The adopted control scheme follows the approach of [12], [25] by applying the inverse of the modified Prandtl-Ishlinskii (MPI) model of the system's response, to the command signal. The MPI model offers good handling of asymmetries in the hysteresis loop, approximating hysteretic nonlinearities with a linearly weighted superposition of $n+1$ backlash operators, with magnitudes of r_i (where $0 \leq i \leq n$) and weight values of w_{hi}, and in series with a linearly weighted superposition of $2m+1$ one-sided dead-zone operators of different thresholds d_j (where $-m \leq j \leq m$) and weight values w_{sj}. Fig. 3b shows the input-output characteristics of these operators. The existence of the inverse MPI model is true under specific conditions and, like the original MPI model, has $n+1$ backlash operators and $2m+1$ one-sided dead-zone operators, characterized by a respective set of parameters, i.e., w'_{hi}, r'_i, w'_{sj}, and d'_j.

As detailed in [26], our closed-loop position control methodology, which is based on the approach of [12], [25], employs first open-loop response data to calculate the MPI model H of the arm's response and its inverse H^{-1}. The feedforward term H^{-1} is then combined with a proportional-integral (PI) feedback controller with anti-windup, which

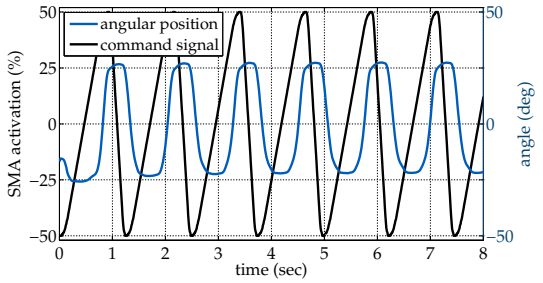

Fig. 4: Open loop response of the joint angular position to a sculling-shaped SMA activation command input.

utilizes the angular position feedback signal from a joint potentiometer (Fig. 2). Normalization of the hysteresis' compensator input and the output signals, via the gains K_{in} and K_{out} in the feedforward path, allows scaling of the reference angular position to the control input range. SMA overheating is avoided by assigning, through the "limiter" block, to the activation signal suitable constraints, here specified so that the PWM duty cycle does not exceed 60%.

B. Experimental results for a single SMA-actuated arm

The primary arm motion profile that was implemented here, is based on a two-stroke pattern, termed *sculling* [14]–[17], which emulates the kinematics of octopus arm-swimming behavior. It involves a velocity ratio β between a slow recovery stroke (opening part) and a faster power stroke (closing part) of the arms. The angular trajectory of the SMA-actuated joint is then implemented according to the acceleration profile described in [15], characterized by the following motion parameters: the angular offset ψ, the angular amplitude A, and the maximum angular velocity of the recovery stroke ω. The total duration of one sculling period of motion is $T_s = T_p + T_r$, with $T_p = 2.5A/(\beta\omega)$ and $T_r = \beta T_p$ being, respectively, the power and recovery time durations. That makes $T_s = (\beta + 1)T_p$.

Following the control scheme described in Section II-A, Fig. 4 shows results from the system's open loop response to SMA activation with such a sculling signal. The plot demonstrates the effects of hysteresis and asymmetry, which result in the output trajectory deviating significantly from the sculling profile. These input-output data were used to calculate the MPI model H and its inverse H^{-1}. The performance attained under the combined feedback-feedforward control scheme, implemented as per Fig. 2 at a $100\,\mathrm{Hz}$ rate, with the PI gains set to $k_p = 3.0$ and $k_i = 0.03$, is shown in Fig. 5. The angular position of the SMA-actuated arm can be seen to track effectively the reference signal (a sculling profile with $A = 15°$, $\psi = 0°$, $\omega = 40°/\,\mathrm{sec}$ and $\beta = 3$), with the exception of a relatively small overshoot that occurs at the end of the power stroke. We also note that the response is quite fast, and exhibits minimal lag with respect to the reference, indicating successful cancellation of the hysteresis.

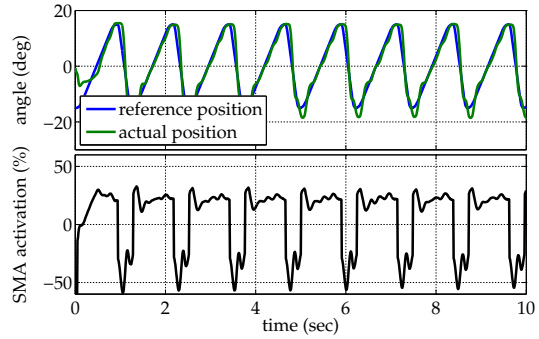

Fig. 5: Tracking of a reference sculling trajectory by the SMA-actuated joint under the combined feedback-feedforward control scheme. The lower graph shows the control signal.

III. TWO-ARM ROBOT SWIMMER

A. Simulation studies

Utilizing computational fluid dynamics (CFD) methodologies, we examined in simulation a two-arm swimmer (Figs. 6), modeled after the robotic prototype of Section III-B. The geometries of the arms are identical to those used in the robot and the swimmer is tested at a stationary position, for rigidly moving arms (with and without non-folding flaps), undergoing the two-stroke sculling motion ($A = 5°$, $\psi = 10°$, $\omega = 10°/\,\mathrm{sec}$ and $\beta = 3$). The details of

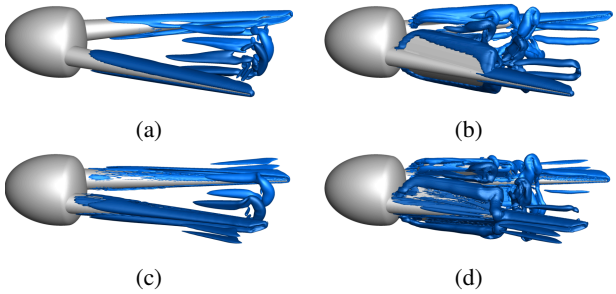

Fig. 6: Hydrodynamic simulations of a two-arm swimmer, modeled after the robotic prototype of Section III-B. Vortical patterns are depicted in blue in the near wake of rigidly moving arms (a,c) without flaps and (b,d) with flaps. (a,b) Recovery stroke. (c,d) Power stroke.

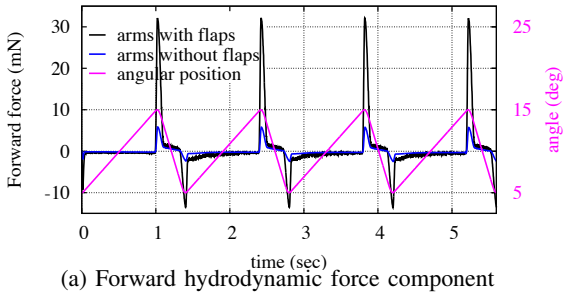

(a) Forward hydrodynamic force component

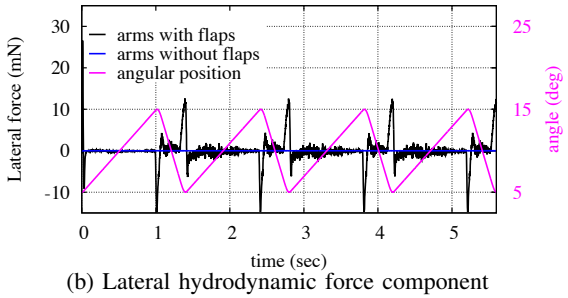

(b) Lateral hydrodynamic force component

Fig. 7: (a) Forward and (b) lateral hydrodynamic force generated by the two-arm system, for arms with and without flaps.

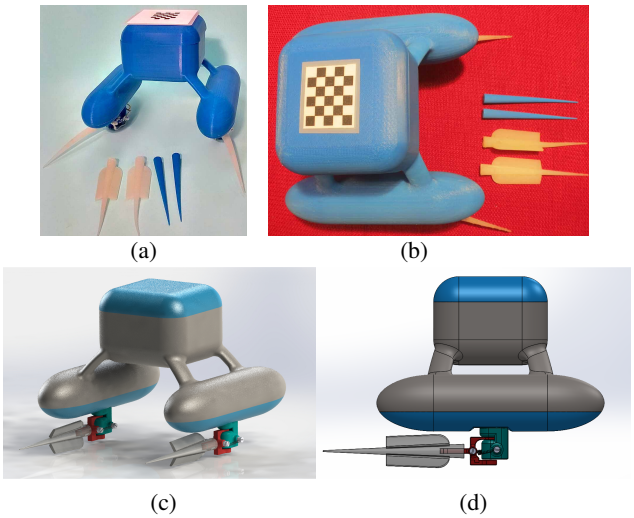

Fig. 8: The two-arm robotic prototype with compliant rotary joints performing sculling. (a) Rear view. All pairs of rigid and silicone arms used in the experiments are shown, with and without flaps. (b) Top view of the two-hull catamaran. (c-d) CAD schematic of the robot with the arms with flaps: (c) rear, and (d) side views.

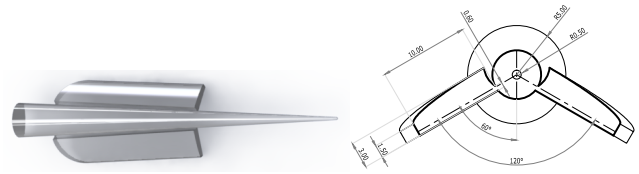

Fig. 9: CAD schematic of the silicone arm with flaps.

the CFD methods, as well as further related results, can be found in [19], [20], [27].

Fig. 6 depicts the fluid field, exhibiting unstructured vortical flow, developed around the rotating arms. The CFD simulations were used to evaluate the total force components (along the swimmer's axis and in the lateral, in-plane direction; Fig. 7) for the two-arm system, and under the effect of flaps. They confirm the generation of a propulsive forward thrust, which is higher than for single-arm systems [18], [21], and considerably increases for arms with flaps (5.6-fold difference in the peak values, Fig. 7a). More importantly, the lateral force is, on average, nearly zero for the two-arm system, in both arm geometries (Fig. 7b), compared to a substantial lateral force for equivalent one-arm systems.

B. SMA-actuated robotic prototype swimmer

Based on the results of the modeling studies, a robotic prototype of a two-arm swimmer (Fig. 8), was fabricated as a proof-of-concept design for soft actuation via SMA springs. The prototype has a rigid body resembling a twin-hull catamaran, and two compliant arms, mounted on the underside of each hull via 1-dof compliant rotary joints, which are actuated by antagonistic pairs of SMA springs, as described in Section II-B. The body is fabricated by ABSplus material, in a 3D printer (Dimension Elite, Stratasys, USA). Each hull, of dimensions $180\,\mathrm{mm}$ x $45\,\mathrm{mm}$ x $45\,\mathrm{mm}$, is cylindrical, with its two edges shaped as prolate hemispheroids, in order to reduce hydrodynamic resistance. The axis-to-axis distance

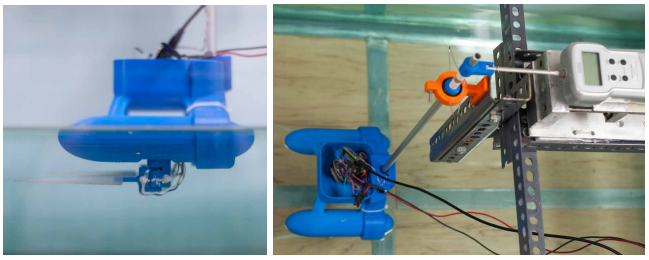

Fig. 10: Set-up for force measurements.

between the parallel streamlined hulls is $140\,\mathrm{mm}$. At $30\,\mathrm{mm}$ above the hulls' axes, lies a rectangular ($90\,\mathrm{mm}$ x $95\,\mathrm{mm}$ x $70\,\mathrm{mm}$) superstructure that houses the electronics and the battery. The SMA-actuated joints are mounted on the middle of the bottom face of each hull, at a position parallel to the direction of swimming; in total, the design can accommodate 6 discrete offset positions with respect to the direction of motion, at every $30°$. The overall dimensions of the prototype are $180\,\mathrm{mm}$ in length, $140\,\mathrm{mm}$ in width, and $122.5\,\mathrm{mm}$ in height, of which approximately $35\,\mathrm{mm}$ are submerged. The overall weight of the robot without the arms is $331\,\mathrm{gr}$.

Apart from the silicone arms described in the previous Section (weighing $3\,\mathrm{gr}$ each), a pair of ABSplus-made arms ($2\,\mathrm{gr}$ each) was also tested with the swimmer (referred to as "rigid"), as well as a second pair of silicone arms ($7\,\mathrm{gr}$ each), incorporating a pair of novel design "flaps", symmetrically positioned at the lateral sides of the arm's axis and at an angle of $120°$ between them (Fig. 9). The flaps' design features thinner layers of material along their junction with the arms, allowing the flaps to almost align with the flow during the recovery stroke of the motion (minimizing, therefore, the induced fluid drag force), while hindering them from reversing during the power stroke (increasing, hence, the projected body area to the flow and maximizing the induced drag). This body-drag difference between power and recovery stroke is meant to enhance the propulsive force generated by the sculling profile, as described in [14]. Although this strategy unavoidably imposes unequal workload on the antagonistic SMAs of the soft joint, the experiments demonstrated good SMA behavior. These flaps emulate, to some extent, the web between the arms of the octopus [14].

The robot is fully untethered and energetically autonomous, being powered by a Li-Po battery located inside the superstructure. The latter also houses the microcontroller platform that controls the two SMA-actuated joints, as well as the associated power electronics (see Section II-A). Wireless communication between the microcontroller and a host PC is implemented via a bluetooth link.

The prototype was tested inside a water tank with dimensions $200\,\mathrm{cm}$ x $70\,\mathrm{cm}$ x $60\,\mathrm{cm}$. Its position and orientation was tracked with a high-definition camera, via computer vision methods, using a checkerboard marker of known size, placed on top of the superstructure (Fig. 8b). Following the motion profile described in Section II-B, several different gaits can be generated from the combination of the two arms, for both forward [15] and turning [16] maneuvers. In this work, we examine gait G1 [15], in which both arms move

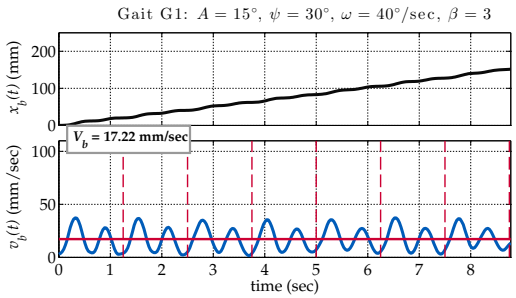

(a) Rigid arms

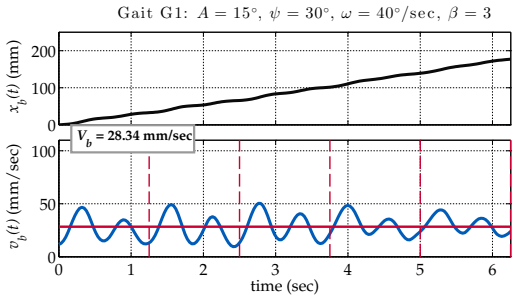

(b) Compliant arms without flaps

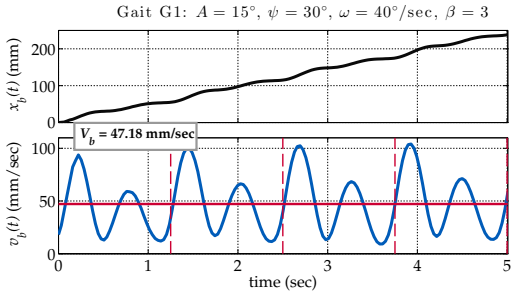

(c) Compliant arms with folding flaps

Fig. 11: Experimental results with closed-loop control: Forward propulsion attained with (a) rigid or (b-c) compliant arms, (b) without and (c) with folding flaps, for swimming with sculling gait $G1$ ($A = 15°$, $\psi = 30°$, $\omega = 40°/\text{sec}$ and $\beta = 3$). In each subfigure, the upper plot shows the robot's displacement and the lower plot the corresponding velocity profile, over a time span of several sculling periods (where $T_s = 1.25$sec). The red horizontal line in the lower plot indicates the average steady-state velocity V_b.

in synchrony.

Force measurements on the robot are performed with a custom test-rig, shown in Fig. 10, and acquired with a high-precision digital force gauge (Alluris FMI-210A5).

C. Experimental results

Experiments with the two-arm robotic swimmer, performing the sculling profile described in [14], demonstrated the generation of forward propulsion via soft, SMA-actuated 1-dof rotary joints, employing the proposed control scheme. The accurate and robust tracking of the arms' reference trajectories, afforded by the closed-loop controller, contributed significantly to the effective mutual cancellation of the side forces generated by the two arms, to ensure the straight-line propulsion of the vessel with minimal yawing motions (footage in accompanying video).

Indicative results for the simplified arms (rigid and compliant) and the arms with flaps, are shown, respectively, in

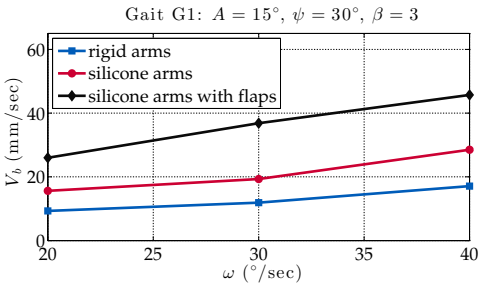

Fig. 12: Average swimming velocity V_b, shown as a function of the recovery stroke velocity ω, of the two-arm SMA-actuated prototype, under closed-loop control, for the three different arm designs.

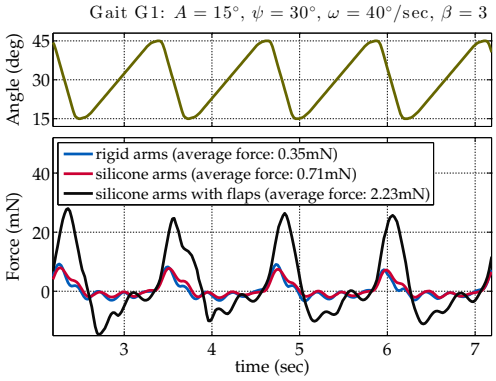

Fig. 13: Lower plot: Instantaneous thrust force generated by the two-arm SMA-actuated prototype, under closed-loop control, for the three different arm designs, shown over four periods of the reference sculling trajectory (shown in the upper plot).

Figs. 11a, b and c, for $A = 15°$, $\psi = 30°$, $\omega = 40°/\text{sec}$ and $\beta = 3$. The instantaneous velocity exhibits periodic variations, induced by the two-stroke sculling motion, with distinct peaks, corresponding to the power stroke, being more evident for the arms with flaps.

As shown in Fig. 12, the robot's average steady-state speed V_b, was found to increase with the angular velocity ω, for all of the three arm designs tested. The maximum V_b value attained with the soft arms with flaps, for $A = 15°$, $\psi = 30°$, $\omega = 40°/\text{sec}$ and $\beta = 3$, was around $47\,\text{mm}/\text{sec}$, significantly higher than the corresponding ones for both the simple compliant arms ($28\,\text{mm}/\text{sec}$) and the rigid arms ($17\,\text{mm}/\text{sec}$). The fact that the latter were found to be the least effective ones can be attributed to the increased loading for rotation of non-compliant arms, which hinders accurate tracking of the prescribed profile.

These findings correlate well with the results of the force measurements (Fig. 13), obtained with the setup in Fig. 10. It can be seen that the propulsive forces developed by the arms with flaps are considerably higher than those of both the plain silicone and rigid arms. The data in Fig. 13 also indicate that the positive thrust peak (reaching values of around $28\,\text{mN}$ in the case of the arms with the flaps) occurs during the arms' power stroke, while negative forces, of a lower peak value, are generated as the recovery stroke is initiated. It should be noted that these observations are in close agreement with the results of the CFD simulations (cf. Fig. 7a).

IV. DISCUSSION AND CONCLUSIONS

This work provides evidence of the feasibility of compliant reduced-size actuation for a two-arm underwater robot swimmer, and other analogous soft robots, based on pairs of antagonistic SMA springs in each joint. Moreover, it highlights the importance of closed-loop control schemes to compensate hysteretic phenomena and asymmetries, and drive the SMAs fast and accurately, and with relatively low computational cost. Propulsive speeds of up to about 0.5 arm lengths per second ($\sim 50\,\mathrm{mm}\,/\,\mathrm{s}$) and forces up to $30\,\mathrm{mN}$ were demonstrated. This performance was found to come at the expense of the SMAs' usable life span: due to the high workload demand on our trained SMAs (approximately $1.05\,\mathrm{V}\,/\,\mathrm{cm}$ for each SMA), they showed aging effects as early as about 1000 cycles, as opposed to the 10000 cycles quoted by the manufacturer for a workload of $0.3\,\mathrm{V}\,/\,\mathrm{cm}$.

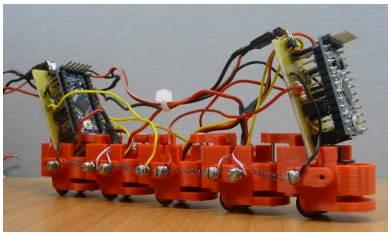

Fig. 14: Five-segment undulatory robot with compliant actuation elements based on SMA springs.

Future work will consider the development of fully-submerged multi-arm swimmers, both with compliant bodies, as well as with compliant actuation elements. Other bio-inspired robot morphologies, like a five-segment undulatory crawler, are also under development, using a similar actuation and control scheme (Fig. 14).

V. ACKNOWLEDGMENT

The authors would like to thank X. Zabulis and P. Pandeleris for their assistance with computer vision issues. Also, the CaSToRC and PRACE-3IP PARADOX HPC clusters (Projects pro14a108 and FP7 RI-312763-12DECI0048).

REFERENCES

[1] D. Trivedi, C. D. Rahn, W. M. Kier, and I. D. Walker, "Soft robotics: Biological inspiration, state of the art, and future research," *Appl. Bion. Biomech.*, vol. 5, no. 3, pp. 99–117, 2008.

[2] A. Albu-Schäffer, O. Eiberger, M. Grebenstein, S. Haddadin, C. Ott, T. Wimböck, S. Wolf, and G. Hirzinger, "Soft robotics," *IEEE Robot. Automat. Mag.*, vol. 15, no. 3, pp. 20–30, 2008.

[3] J. M. Jani, M. Leary, A. Subic, and M. A. Gibson, "A review of shape memory alloy research, applications and opportunities," *Mater. Design*, vol. 56, no. 0, pp. 1078 – 1113, 2014.

[4] S. Kim, E. Hawkes, K. Cho, M. Jolda, J. Foley, and R. Wood, "Micro artificial muscle fiber using NiTi spring for soft robotics," in *IEEE/RSJ Int. Conf. Int. Rob. Syst. (IROS)*, 2009, pp. 2228–2234.

[5] Y. P. Lee, B. Kim, M. G. Lee, and J.-O. Park, "Locomotive mechanism design and fabrication of biomimetic micro robot using shape memory alloy," in *IEEE Int. Conf. Rob. Autom. (ICRA)*, 2004, pp. 5007–5012.

[6] A. Menciassi, S. Gorini, G. Pernorio, and P. Dario, "A SMA actuated artificial earthworm," in *IEEE Int. Conf. Rob. Autom. (ICRA)*, vol. 4, 2004, pp. 3282–3287.

[7] H. Yuk, J. H. Shin, and S. Jo, "Design and control of thermal SMA based small crawling robot mimicking *C. elegans*," in *IEEE/RSJ Int. Conf. Int. Rob. Syst. (IROS)*, 2010, pp. 407–412.

[8] S. Seok, C. Onal, K.-J. Cho, R. Wood, D. Rus, and S. Kim, "Meshworm: A peristaltic soft robot with antagonistic nickel titanium coil actuators," *IEEE/ASME Trans. Mechatron.*, vol. 18, no. 5, pp. 1485–1497, 2013.

[9] M. Calisti, M. Giorelli, G. Levy, B. Mazzolai, B. Hochner, C. Laschi, and P. Dario, "An octopus-bioinspired solution to movement and manipulation for soft robots," *Bioinsp. Biomim.*, vol. 6, no. 3, p. 036002, 2011.

[10] Z. Wang, G. Hang, J. Li, Y. Wang, and K. Xiao, "A micro-robot fish with embedded SMA wire actuated flexible biomimetic fin," *Sensor Actuat. A-Phys.*, vol. 144, no. 2, pp. 354 – 360, 2008.

[11] M. Follador, M. Cianchetti, A. Arienti, and C. Laschi, "A general method for the design and fabrication of shape memory alloy active spring actuators," *Smart Mater. Struct.*, vol. 21, no. 11, p. 115029, 2012.

[12] K. Kuhnen, "Modeling, identification and compensation of complex hysteretic nonlinearities: A modified Prandtl-Ishlinskii approach," *Eur. J. Control*, vol. 9, no. 4, pp. 407–418, 2003.

[13] M. Sfakiotakis, A. Kazakidi, and D. P. Tsakiris, "Octopus-inspired multi-arm robotic swimming," *Bioinsp. Biomim.*, vol. 10, no. 3, p. 035005, 2015.

[14] M. Sfakiotakis, A. Kazakidi, A. Chatzidaki, T. Evdaimon, and D. P. Tsakiris, "Multi-arm robotic swimming with octopus-inspired compliant web," in *IEEE/RSJ Int. Conf. Int. Rob. Syst. (IROS)*, Chicago, Illinois, USA, 2014, pp. 302–308.

[15] M. Sfakiotakis, A. Kazakidi, N. Pateromichelakis, and D.P. Tsakiris, "Octopus-inspired 8-arm robotic swimming by sculling movements," in *IEEE Int. Conf. Rob. Autom. (ICRA)*, Karlsruhe, Germany, 2013, pp. 5135–5141.

[16] M. Sfakiotakis, A. Kazakidi, and D. P. Tsakiris, "Turning maneuvers of an octopus-inspired multi-arm robotic swimmer," in *IEEE Med. Conf. Control Autom. (MED)*, Greece, 2013, pp. 1343–1349.

[17] M. Sfakiotakis, A. Kazakidi, N. Pateromichelakis, J.A. Ekaterinaris, and D.P. Tsakiris, "Robotic underwater propulsion inspired by the octopus multi-arm swimming," in *IEEE Int. Conf. Rob. Autom. (ICRA)*, St. Paul, USA, 2012, pp. 3833–3839.

[18] A. Kazakidi, V. Vavourakis, D. P. Tsakiris, and J. Ekaterinaris, "A numerical investigation of flow around octopus-like arms: near-wake vortex patterns and force development," *Comp. Meth. Biomech. Biomed. Eng.*, vol. 18, no. 12, pp. 1321–1339, 2015.

[19] A. Kazakidi, D. P. Tsakiris, F. Sotiropoulos, and J. A. Ekaterinaris, "A computational fluid dynamic study of intense cephalopod-like motions," in *44th AIAA Fluid Dynamics Conference*, Atlanta, USA, 2014, pp. 1–15.

[20] A. Kazakidi, D.P. Tsakiris, F. Sotiropoulos, and J.A. Ekaterinaris, "Numerical investigation of aquatic locomotion with cephalopod-like appendages," in *19th Congress of the European Society of Bioengineering (ESB)*, Patra, Greece, 2013.

[21] A. Kazakidi, V. Vavourakis, N. Pateromichelakis, J.A. Ekaterinaris, and D.P. Tsakiris, "Hydrodynamic analysis of octopus-like robotic arms," in *IEEE Int. Conf. Rob. Autom. (ICRA)*, St. Paul, USA, 2012, pp. 5295–5300.

[22] V. Vavourakis, A. Kazakidi, D.P. Tsakiris, and J.A. Ekaterinaris, "A nonlinear dynamic finite element approach for simulating muscular hydrostats," *Comput. Methods Biomech. Biomed. Engin.*, vol. 17, no. 8, pp. 917–931, 2014.

[23] V. Vavourakis, D. Bampasakis, A. Kazakidi, N. Pateromichelakis, J.A. Ekaterinaris, and D.P. Tsakiris, "Generation of primitive behaviors for non-linear hyperelastic octopus-inspired robotic arm," in *IEEE Int. Conf. Biomed. Rob. Biomech.*, Roma, Italy, 2012, pp. 725–730.

[24] Y. H. Teh and R. Featherstone, "An architecture for fast and accurate control of shape memory alloy actuators," *Int. J. Rob. Res.*, vol. 27, no. 5, pp. 595–611, 2008.

[25] J.-C. Shen, W.-Y. Jywe, H.-K. Chiang, and Y.-L. Shu, "Precision tracking control of a piezoelectric-actuated system," in *IEEE Med. Conf. Control Autom. (MED)*, 2007, pp. 1–6.

[26] T. Evdaimon, M. Sfakiotakis, and D. P. Tsakiris, "A closed-loop position control scheme for sma-actuated joints," in *IEEE Med. Conf. Control Autom. (MED)*, Palermo, Italy, 2014, pp. 1527–1532.

[27] A. Kazakidi, D. P. Tsakiris, D. Angelidis, F. Sotiropoulos, and J. A. Ekaterinaris, "CFD study of aquatic thrust generation by an octopus-like arm under prescribed deformations," *Computers and Fluids*, vol. 115, pp. 54–65, 2015.